Statistics of Echoes From Mixed Assemblages of Scatterers With Different Scattering Amplitudes and Numerical Densities

Wu-Jung Lee and Timothy K. Stanton

***Abstract*—In this paper, an exact solution is derived, evaluated, and numerically validated for describing the statistics of echoes from mixed assemblages of scatterers. Here, a "mixed assemblage" involves the geometry in which there is more than one type of scatterer spatially interspersed and uniformly distributed within the analysis window, which is much larger than the resolution cell of the system (i.e., there are many independent samples per window). The scatterers are generally not resolvable and the signals are narrowband. The scattering geometry is in the backscattering direction in the direct-path case in which there are no interfering echoes from neighboring boundaries. The probability density functions (pdfs) of echo envelopes in such cases can be highly non-Rayleigh and possess heavy tails, and the shape of the pdf curves contains information for characterizing and discriminating the composition of mixed assemblages. The general formulation is based on characteristic functions (CFs; hereafter referred to as the CF-based mixed assemblage pdf) and incorporates effects due to the scatterers being randomly located in the beam. Comparisons are made between the performance of the CF-based mixed assemblage pdf and the commonly used mixture model for simulated cases involving two different types of scatterers, arranged either interspersed or segregated in the analysis window. Both models can be made to fit the shape of the echo pdf of simulated data in some conditions. However, mismatch between model assumptions and the actual physical scattering processes can lead to order of magnitude errors in the inferred numerical density and backscattering amplitude of each type of scatterers.**

***Index Terms*—Echo statistics, mixed assemblage, scattering.**

I. Introduction

THE ability to accurately characterize and discriminate between the echoes from various sources of scattering is crucial to many radar and sonar systems [1]. When a sonar/radar beam scans through a volume or across a surface of interest, the echoes fluctuate as a result of the variation of scatterer composition, orientation, location within the beam, and numerical density, all of which are random variables. The statistics of the echoes provide an avenue to infer key properties of the scatterers. For example, the shape of the probability density functions (pdfs) can be used to estimate the numerical density of the scatterers [2], [3]. Furthermore, understanding these pdfs is important in predicting sonar/radar performance when discriminating between a target of interest and clutter [4], [5].

When the resolution cell of a sonar/radar system contains a large number of scatterers, the central limit theorem holds for the real (in-phase) and imaginary (quadrature) components of the echoes, and the amplitudes of echo envelopes (or, more precisely, the magnitude of the complex echo) are Rayleigh distributed, a direct consequence of the real and imaginary components being Gaussian [6]. When any one of the above conditions is not satisfied, non-Rayleigh-distributed echoes with heavy tails can occur. The "tail" is defined for the region where the values of the echo amplitude are relatively high and probability densities are relatively low. When the resolution cell contains only a small number of scatterers, the resultant echo amplitude pdf (hereafter referred to as the "echo pdf") is highly non-Rayleigh, owing significantly to the random weighting factors due to random locations of the scatterers in the beam. The distribution associated with this echo amplitude modulation is termed the "beampattern pdf" [7], [8] and this (beampattern) effect is one of the primary factors for non-Rayleigh-distributed echoes.

Another common reason for non-Rayleigh-distributed echoes to occur is when there is more than one type of scatterer in the aggregation included in the analysis window (where the analysis window is much larger than the resolution cell of the system, resulting in many statistically independent samples within the window). In this case, the echo pdf can be non-Rayleigh even when the total number of scatterers is large. Here, the same "type" of scatterers refers to scatterers with the same scattering amplitude (or, if it is a random variable, the same amplitude distribution with the same mean amplitude) at the frequency under consideration. For example, the analysis window could contain only a few strong scatterers interspersed within a large number of scatterers of another type, which has a much smaller scattering amplitude. Without the strong scatterers, the echoes would be Rayleigh distributed due to the relatively weak scatterers. However, if the echo from the strong scatterers is large

Manuscript received June 18, 2012; revised May 01, 2013; accepted September 26, 2013. Date of publication January 13, 2014; date of current version October 09, 2014. This work was supported by two National Oceanographic Partnership Program (NOPP) projects through the U.S. Office of Naval Research (ONR), as well as the Academic Programs Office at the Woods Hole Oceanographic Institution.

Associate Editor: D. A. Abraham.

W.-J. Lee was with the Department of Applied Ocean Physics and Engineering, Woods Hole Oceanographic Institution, Woods Hole, MA 02543-1053 USA. She is now with the Institute for Systems Research, University of Maryland, College Park, MD 20740 USA (e-mail: wjlee@umd.edu).

T. K. Stanton is with the Department of Applied Ocean Physics and Engineering, Woods Hole Oceanographic Institution, Woods Hole, MA 02543-1053 USA (e-mail: tstanton@whoi.edu).

Color versions of one or more of the figures in this paper are available online at http://ieeexplore.ieee.org.

Digital Object Identifier 10.1109/JOE.2013.2285657

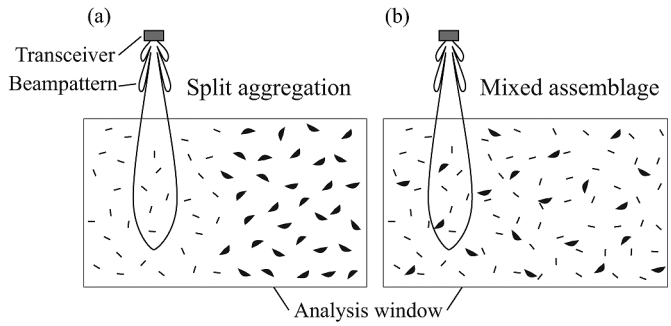

Fig. 1. Illustration of analysis windows containing two possible spatial arrangements for aggregations composed of more than one type of scatterer. (a) Split aggregation: scatterers of different types are separated into their own subregions. (b) Mixed assemblage: scatterers of different types are uniformly interspersed throughout the analysis window. In each case, the sonar/radar resolution cell is much smaller than the analysis window and, in case (a), it is also much smaller than each subregion.

enough so that it is comparable to or larger than the collective echo from the weak scatterers, its presence can significantly influence the statistics, increasing the tail and making it non-Rayleigh. This type of condition is prevalent in nature such as in the cases of the presence of occasional large fish foraging in a zooplankton patch [3], [9], sparsely distributed rock outcrops on a bed of sand ripples on the seafloor [10], bubble plumes from occasional breaking waves under a rough sea surface [11], isolated or small groups of trees in a field of bushes or grassland [12], etc.

The size of the sonar/radar resolution cell relative to the size and spatial distributions of the scatterers determines the process by which the scatterers are "seen" by the system through the sonar/radar beam and consequently affects the formulation of appropriate echo statistic models. For example, the spatial distribution concerning two different types of scatterers in an aggregation can be simplified into two distinct cases, one in which the two types are separated into subregions [Fig. 1(a)] and the other in which the two types are interspersed [Fig. 1(b)]. In each case, the size of the resolution cell of the sonar/radar system is much smaller than the size of the analysis window and, in the first case, also much smaller than the size of each subregion. Thus, in the first case, in any one ping, only one type of scatterer is covered by the sonar/radar beam [Fig. 1(a)]. As a result, the echo statistics for the pings included in the analysis window containing both subregions are nonstationary across the two subregions and, therefore, form a "split aggregation" [13], [14]. The second case involves the "mixed assemblage," which is the focus of this paper [Fig. 1(b)]. Here, the two types of scatterers are interspersed and uniformly distributed so that the echo statistics within the analysis window are stationary. However, note that if the size of the resolution cell is further reduced so that it is much smaller than the spacing of the scatterers, the sonar/radar beam will go through many transitions between the two types of scatterers within the analysis window. In this case, the statistics of echoes are equivalent to those in the case of split aggregations instead of mixed assemblages.

Many models have been proposed to characterize non-Rayleigh-distributed echoes. Statistical analysis of data usually involves fitting the data to a large pool of models to determine the best representation (e.g., [4], [5], [15], and [16]). However, since most of these models do not provide explicit connections between the model parameters and the underlying scattering mechanisms, statistical descriptions using this data-driven approach are often only applicable to data collected using similar systems in specific geographical locations. In other words, these models are neither predictive nor interpretive with respect to the variation of sonar/radar system parameters or the scattering processes in the environment.

Several other models [14], [17]–[19] do provide a link between the model parameters and the physical scattering environment by imposing specific assumptions on the scatterers in a resolution cell. Among them, the K-distribution has been successfully applied to data collected under a variety of contexts [17], [20]. However, the link between the K-distribution model parameters and the environment was established under the assumption that the scattering amplitude of scatterers or scattering patches after the beampattern effects is exponentially distributed [19]. This assumption is not realistic for many important scenarios in nature, including most biological aggregations in the sea [21].

Recognizing the potential nonstationarity of echo samples included in the analysis window [as in the split aggregation represented in Fig. 1(a)], the multiple-component mixture model (referred to as the "M-component mixture model" throughout this paper) has been used extensively to fit experimental data (e.g., [13], [16], and [22]–[25]). This model describes the echo distribution as a linear combination of multiple probability distributions through

$$p_A^{\Sigma}(a) = \sum_{m=1}^{M} w_m p_{A,m}(a) \tag{1}$$

where a is the echo amplitude (or, more precisely, magnitude of complex echo), M is the number of component pdfs, and $p_{A,m}(a)$ and w_m are the pdf and proportional factor of the mth component pdf, respectively, with the constraint $\sum_{m=1}^{M} w_m = 1$.

Specifically for split aggregations composed of more than one type of scatterer, each being in their own subregion, M denotes the number of subregions in the aggregation, and the proportional factor w_m is determined by the relative proportion of data included in the analysis window from the mth subregion. Each component pdf can be written as

$$p_{A,m}(a) = p_{A,m}(a; N_m, r_m) \tag{2}$$

where N_m and r_m are the number of scatterers and relative scattering amplitude, respectively, of the mth type of scatterer. Note that each N_m refers to the number of the mth type of scatterers in the *half-space*. Therefore, once weighted by the beampattern, the *effective* number of scatterers (i.e., the number of scatterers approximately within the resolution cell) will be much smaller. Each r_m is calculated relative to the amplitude of the weakest scatterer in the aggregation. The scattering from this type of aggregation is conceptually analogous to the scenario proposed by Crowther [14], where the seafloor patches insonified by the sonar beam alternate between two types of seabed substrates.

However, for mixed assemblages as depicted in Fig. 1(b), each echo sample is formed by a coherent sum of the echoes

from each scatterer (regardless of type) [8]. Therefore, instead of a weighted sum over several component pdfs, the resultant echo pdf should be evaluated through a coherent summation of complex random variables, each associated with a scatterer. The echo pdf can be written in the following parametrized form:

$$p_A^{\Sigma}(a) = p_A^{\Sigma}(a; N_1, N_2, \ldots, N_M, r_1, r_2, \ldots, r_M). \quad (3)$$

In this study, the echo statistics associated with mixed assemblages [as represented in Fig. 1(b)] are formulated with this approach of coherently adding all echoes. This is a physics-based approach, beginning with the scattering physics of individual scatterers and incorporating effects due to their locations in the beam. Both the scattering by individuals and their locations in the beam are randomized. This is in contrast to the aforementioned approaches in which parameters of the echo statistics are not directly linked to the physical processes. The new formulation is a specialized version of the general formula for the echo pdf of an arbitrary number of scatterers given in [8], which utilized the method of characteristic functions (CFs) proposed by Barakat [26] to calculate the envelope pdf of the sum of random variables. The signals are narrowband and are modeled as continuous waves. The aforementioned beampattern effects are also incorporated explicitly in this formulation [7]. Theoretical predictions made by this CF-based mixed assemblage pdf are validated by numerical simulations of echoes from mixed assemblages.

In addition, the performance of the CF-based mixed assemblage pdf as an inference tool is compared with that of the M-component mixture model in the cases of both split aggregations and mixed assemblages containing two types of scatterers (Fig. 1) over a wide range of numerical densities and relative scattering amplitudes of the scatterers [N_m's and r_m's in (2) and (3)]. Through a best-fit analysis involving maximum-likelihood estimators (MLEs), it is observed that only when model assumptions correspond with the physical scattering processes can the models simultaneously fit the shape of the echo pdf of simulated data and accurately infer the parameters of the composition of simulated split aggregations and mixed assemblages. The mismatch between the model and the scattering physics can result in significant errors in parameter estimates under important conditions.

This paper is organized as follows. In Section II, the theoretical development of the CF-based mixed assemblage pdf and the incorporation of beampattern effects are presented. In Section III, the procedures of generating theoretical curves and numerical simulations are discussed, and important examples of numerically validated CF-based mixed assemblage pdfs are shown. The performances of the CF-based mixed assemblage pdf and the M-component mixture model as inference tools are compared in Section IV. The summary and conclusion of this study are given in Section V.

II. Theoretical Development of CF-Based Mixed Assemblage PDF

In this section, a general expression is derived to describe the echo pdf for mixed assemblages as a function of the numerical density and scattering amplitude of each type of scatterer, as well as the number of scatterer types. This expression is general and applicable to the case in which the scatterers are of arbitrary type. The derivation follows the method of CFs [26] to obtain the envelope statistics for the sum of generic complex random variables. The beampattern effects, which are of particular concern for radar/sonar applications, are also incorporated explicitly in the formulation [7], [8]. Some derivations from previous works are summarized here as they will be drawn from in the final formulation.

A. Problem Setup

In a mixed assemblage, different types of scatterers are uniformly interspersed among one another, as depicted in Fig. 1(b). The geometry involves direct paths between the radar/sonar and the scatterers in the backscattering direction, with no reflections from the boundaries such as the seafloor and sea surface.

Assuming the use of narrowband signals, the echo voltage V_i received through the sonar/radar system associated with each scatterer can be modeled as a narrowband continuous-wave signal and described in a (complex) phasor form

$$V_i = a_i e^{j(\theta_i + \omega_a t)} \quad (4)$$

where ω_a is the angular frequency, $j = \sqrt{-1}$, and a_i and θ_i are the random variables describing the echo magnitude and relative phase associated with the ith scatterer, respectively. All a_i and θ_i are statistically independent. The magnitude of each echo a_i depends upon the size, shape, orientation, and material properties of the ith scatterer, as well as the frequency and the location of the ith scatterer in the beam. The dependence of a_i on the location of the ith scatterer in the beam is implicit here, and will be given in detail in Section II-C. Since the path differences induced by the positions of the scatterers are assumed to be greater than the wavelength of the incident wave, and the locations of the scatterers are assumed to be random and independent of one another, θ_i can be modeled as a random variable uniformly distributed over the range of $[0, 2\pi)$. The range resolution modeled here spans the entire half-space owing to the continuous-wave assumption. However, the model is applicable to narrowband systems of which the range resolution is determined by the length of the transmitted signal. In such cases, the number of scatterers in the beam discussed in this paper can be converted to the numerical density.

For the case of N scatterers randomly located in the half-space insonified/irradiated by the sonar/radar beam, the total echo (voltage) measured through the system V^{Σ} can be expressed as a sum of the contributions from individual scatterers, i.e.,

$$V^{\Sigma} = \sum_{i=1}^{N} V_i = e^{j\omega_a t} \sum_{i=1}^{N} a_i e^{j\theta_i}. \quad (5)$$

Since the scatterers are located both in the mainlobe, sidelobes, and nulls of the beam, the number of scatterers effectively insonified/irradiated through the corresponding weighting of the beampattern is generally much lower than N. The echo pdf analyzed in this paper deals with fluctuations of envelope amplitude (i.e., magnitude of complex signal) of the total field $a = |V^{\Sigma}|$. Its distribution will be denoted by $p_A^{\Sigma}(a)$ throughout this paper.

For reasons given above, this pdf is a strong function of not only the mainlobe, but also the sidelobes, of the sonar/radar beam.

B. Method of CFs—Beampattern Effects Not Explicit

The above formulation for the total echo measured through a sonar system is the same as the general case described by Barakat [26] in which a finite number of independent sinusoidal waves with arbitrary magnitudes and random phases are summed coherently. He derived a useful formula to express the pdf of the resultant echo magnitude as a Fourier–Bessel series expansion of the product of CFs [27] associated with the pdf of the real or imaginary part of individual phasors. The method is summarized below.

Define y_i to be the real part of the scattering contribution from the ith scatterer and $p_{A_i}(a_i)$ to be the distribution of its magnitude. Since $y_i = \mathrm{Re}\{V_i\} = a_i \cos\theta_i$, y_i can be viewed as the product of two independent random variables a_i and $\cos\theta_i$. Through manipulation of the product of two random variables, the distribution of y_i is shown to be

$$p_{y_i}(y_i) = \begin{cases} \dfrac{1}{\pi}\displaystyle\int_{|y_i|}^{\infty} \frac{p_{A_i}(a_i)}{(a_i^2 - y_i^2)^{1/2}} da_i, & |y_i| \le a_i \\ 0, & |y_i| > a_i. \end{cases} \tag{6}$$

Define y^{Σ} to be the real part of the total echo field $y^{\Sigma} = \mathrm{Re}\{V^{\Sigma}\}$, then its pdf can be expressed as the convolution of pdfs of the real part of individual echoes

$$p_{y^{\Sigma}} = p_{y_1} * p_{y_2} * p_{y_3} * \cdots. \tag{7}$$

Define ϕ_i to be the CF of $p_{y_i}(y_i)$

$$\phi_i(\omega) = \mathrm{FT}\{p_{y_i}(y_i)\} = \int_{-\infty}^{\infty} p_{A_i}(a_i) J_0(\omega a_i) da_i \tag{8}$$

where $\mathrm{FT}\{\cdot\}$ denotes the Fourier transform and $J_\nu(\cdot)$ denotes the cylindrical Bessel function of the first kind of order ν. Intuitively, the Bessel function arises here as a result of representing the scattering amplitudes in the polar coordinates. Since the convolution of pdfs corresponds to the product of CFs, the CF of the pdf of the real part of the total echo field from N scatterers ϕ^{Σ} is

$$\phi^{\Sigma}(\omega) = \prod_{i=1}^{N} \phi_i(\omega). \tag{9}$$

By considering y^{Σ} as a projection of the vector $(\mathrm{Re}\{V^{\Sigma}\}, \mathrm{Im}\{V^{\Sigma}\})$ onto the real axis in the complex plane and using the fact that $\mathrm{Re}\{V^{\Sigma}\}$ and $\mathrm{Im}\{V^{\Sigma}\}$ have the same amplitude distribution, the pdf of the length of this vector $(a = |V^{\Sigma}|)$ can be written in the form of a Fourier–Bessel series

$$p_A^{\Sigma}(a) = 2a \sum_{n=1}^{\infty} \frac{\phi^{\Sigma}\left(\dfrac{\eta_n}{a_{\max}}\right)}{[a_{\max} J_1(\eta_n)]^2} J_0\left(\eta_n \frac{a}{a_{\max}}\right) \tag{10}$$

where $a_{\max}$ is the maximum echo amplitude, and η_n $(n = 1, 2, \ldots)$ are the positive roots of $J_0(x) = 0$. This expression is obtained by approximating ϕ^{Σ} as a band-limited signal and writing the inverse Fourier transform (or the inverse Hankel transform, see discussion in the next paragraph) as a series sum [26]. Equation (6) in this paper corresponds to [26, eq. (13)], (21) corresponds to [26, eq. (21)], and (10) corresponds to [26, eq. (55) and (56)]. The combination of (9) and (10) can be used to calculate the echo pdf of an aggregation of an arbitrary number of scatterers with arbitrary scattering amplitudes.

In the above formulation, the quantity $p_{A_i}(a_i)$ represents the probability that a_i lies between a_i and $a_i + da_i$ in the complex plane, where da_i is an infinitesimal segment in the radial direction on the polar coordinates. By substituting $p_{A_i}(a_i)$ with $\tilde{p}_{A_i}(a_i) \equiv p_{A_i}(a_i)/2\pi a_i$, (8) and (10) can be written as a truncated Hankel transform of order 0 and an inverse Hankel transform, respectively. Although not implemented in this paper, the use of a numerical Hankel transform routine along with these equivalent expressions may greatly improve the efficiency of model calculation [28], [29].

C. Incorporating Beampattern Effects

Since each a_i is measured through the radar/sonar system, the location of the ith scatterer in the beam will determine the weighting factor applied by the radar/sonar system to the scattering amplitude of the echo. These beampattern effects can be explicitly accounted for when forming $p_{A_i}(a_i)$. For a single scatterer randomly located in the beam, the echoes "seen" through the receiver of the system (i.e., including beampattern effects) can be viewed as a product of two random variables s_i and b, where s_i is the magnitude of the scattering amplitude of the ith scatterer (without beampattern effects), and b is the random weighting factor imposed by the beam. The echo envelope pdf of the ith scatterer as measured through the receiver can be expressed as

$$p_{A_i}(a_i) = \int_{a_i}^{\infty} \frac{1}{s_i} p_{S_i}(s_i) p_B\left(\frac{a_i}{s_i}\right) ds_i \tag{11}$$

where $p_{S_i}(s_i)$ is the distribution of the magnitude of the scattering amplitude of the ith scatterer (i.e., the echo amplitude before the beampattern effects), and $p_B(b)$ is the beampattern pdf (originally derived in [7], with subsequent papers summarized in [8]). For a system with an axisymmetric beampattern

$$p_B(b) = \sum_l \frac{p_\Psi(\psi_l(b))}{\left|\dfrac{db}{d\psi}\right|_{\psi_l(b)}} \tag{12}$$

where ψ is a random variable representing the polar angle between the scatterer position and the axis of the beam, and each ψ_l is a root to $b = b(\psi)$. All simulations and analyses carried out in this paper are conducted under the assumption of an axisymmetric circular transceiver aperture with $ka_T = 2\pi$, where k is the wavenumber and a_T is the aperture radius. This corresponds to a beamwidth of approximately 30°. The two-way beampattern of such an aperture is

$$b(\psi) = \left(\frac{2J_1(ka_T \sin\psi)}{ka_T \sin\psi}\right)^2. \tag{13}$$

Equations (11)–(13) are evaluated numerically in this study. Details of the numerical evaluation are discussed in

Appendix A, together with the beampattern $[b(\psi)]$ and beampattern pdf $[p_B(b)]$ of this transceiver, as well as the echo envelope pdf associated with only one scatterer in the beam $[p_A(a; N = 1)]$. For a more complicated beampattern with both polar and azimuthal angular dependence, such as a transceiver with a rectangular aperture, (12) and (13) have to be modified, but the same general formulation in (11) is applicable [7].

D. Echoes From Mixed Assemblages

The above CF-based approach can be used to calculate the echo pdf associated with mixed assemblages through a simple modification of (9). In the mixed assemblage, assume that there are M types of scatterers, each with N_m $(m = 1, 2, \ldots, M)$ scatterers randomly and uniformly distributed in the half-space. Using (9), the CF of the pdf of the real part of the assemblage echo can be expressed as

$$\phi^{\Sigma}(\omega) = \prod_{m=1}^{M} (\phi_m(\omega))^{N_m} \tag{14}$$

where ϕ_m denotes the CF of a single scatterer of type m and can be obtained by (8). The total echo pdf can then be calculated using (10).

The CF-based mixed assemblage pdf calculated using (10) and (14) rigorously incorporates important parameters associated with the system and scatterers: 1) beampattern effects associated with the random locations of the scatterers in the beam; 2) statistics of the random scattering amplitude (before beampattern effects) of each scatterer; and 3) number of each type of scatterer. Each of these parameters is accounted for explicitly.

III. Numerical Validation and Examples of CF-Based Mixed Assemblage PDF

In this section, the theoretical CF-based mixed assemblage pdf derived in Section II is validated by simulated data. The effects of the change of mixed assemblage composition on the shape of the echo pdf are also examined.

A. Model Parameters

The CF-based mixed assemblage pdf derived in Section II is described by three parameters related to the composition of the mixed assemblage: the number of scatterer types M, the number of each type of scatterers N_m, and the *relative*, rather than absolute, scattering amplitudes of the different types of scatterers r_m. The importance of M and N_m is evident in forming the CF of the total mixed assemblage pdf through (14). The importance of r_m is not only important to the echo statistics, but is also closely related to the notion of pdf normalization in this study, as discussed in detail below.

In this study, all echo pdfs are normalized with respect to the root mean square (rms) amplitude of the echo ensemble through the procedure detailed in Appendix B to facilitate data-model comparisons. The normalization procedure allows the analysis to focus on the *shape* of the echo pdf (associated with either individual or aggregation echoes) by removing their dependency on the absolute scattering amplitude of the scatterers and many environment- and system-specific parameters, such as range-dependent transmission loss and system gain. For example, the unnormalized echo pdfs of two aggregations composed of the same number of scatterers with different absolute scattering amplitudes will have the same shape but will be shifted and occupy different locations on the amplitude axis, whereas the normalized echo pdfs of these two aggregations will coincide with each other.

By the same reasoning, for mixed assemblages, it is the *relative* scattering amplitudes, instead of their absolute levels, among the different types of scatterers that are important to the shape of the mixed assemblage echo pdf. As discussed in Section II, the magnitude of the scattering amplitude of each scatterer is specified by a distribution [e.g., $p_{S_i}(s_i)$ for the ith scatterer], instead of a fixed value. The statistics of the scattering amplitude of the mth type of scatterer can be described through the use of the ratio

$$r_m = \frac{\lambda_m}{\lambda_1} \tag{15}$$

where λ_m and λ_1 are the rms magnitudes of the scattering amplitudes (before beampattern effects) of the mth type of scatterer and the weakest scatterer in the assemblage, respectively $(m = 1, 2, \ldots, M; \lambda_M > \lambda_{M-1} > \cdots > \lambda_1)$. In this study, all simulated data and theoretical curves are generated under the assumption that the magnitude of scattering amplitude of each individual scatterer (i.e., the echo before beampattern effects) is Rayleigh distributed, following the convention below

$$p_{S,\mathrm{Rayleigh}}(s; \lambda_m) = \frac{s}{\lambda_m^2} e^{-s^2/2\lambda_m^2}. \tag{16}$$

In this case, λ_m is proportional to the mean of the distribution of the magnitude of the scattering amplitude of the mth type of scatterer. Because the quantity λ_m^2 is a measure of energy, r_m^2 is equal to the ratio of the mean of the backscattering cross section (square of magnitude of scattering amplitude) of the mth type of scatterer to that of the weakest scatterer. All simulation and theoretical echo pdfs in this study are generated by fixing $\lambda_1 = 1$ and varying λ_m. Therefore, r_m is used to substitute for λ_m in all following sections. Furthermore, since $r_1 = 1$ by definition, explicit expression of r_1 is omitted in all following discussions.

To illustrate the effects of a mixed assemblage composition on the shape of the echo pdf, particularly on the non-Rayleigh elevated tail of the pdf, theoretical curves and simulated data are generated for mixed assemblages composed of only two types of scatterers $(M = 2)$. For simplicity, these two types of scatterers will be referred to as "strong" and "weak" scatterers, with the number of each type of scatterer denoted by N_s and N_w, respectively. The ratio r_2 of the magnitudes of the scattering amplitudes of the strong to the weak scatterers is specially denoted by r_{sw} in this case. The phase of each individual scatterer is assumed to be uniformly distributed over the range of $[0, 2\pi)$ for all simulated data and theoretical curves.

B. Simulated Data Generation

Following (16), independent Rayleigh-distributed echoes (before the beampattern effects) are generated from inverse

transform sampling with parameter r_m [as defined in (15)]. The value of λ_1 is fixed at 1 for convenience without loss of generality. The magnitudes of these echoes are further multiplied by the beampattern weighting factor to obtain the echo magnitudes after the beampattern effects. The beampattern weighting factors are determined by the random locations of the scatterers in the beam. In the present case, when a circular aperture is considered, the random location refers to the polar angle (ψ) of the scatterer to the axis of the beam, with a distribution of $p_\Psi(\psi) = \sin\psi$ [27]. The phase of the echo from each individual scatterer is generated by drawing samples from a uniform distribution over the range of $[0, 2\pi)$.

Each independent realization of the ensemble is formed by coherently summing $\sum_{m=1}^{M} N_m$ random phasors with the above magnitudes and phases and taking its envelope (absolute value), which represents an echo from one or more scatterers. The echo pdf of the simulated data is obtained through forming the number frequency histogram of simulated realizations that are also normalized following the procedure described in Appendix B. Note that the echo pdf of simulated data is derived here for the purpose of visual comparison with the theoretical models. Therefore, binning boundaries of the histogram are not critical in the analysis and can be changed for the clarity of visual display.

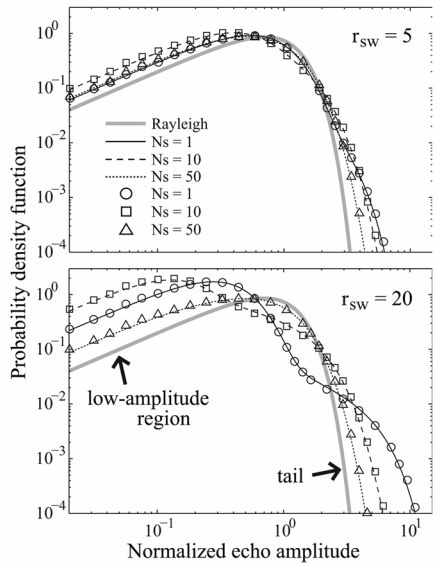

Fig. 2. Validation of the theoretical CF-based mixed assemblage pdf using (10) and (14) (lines) with numerically simulated data (symbols) for the case of two types of scatterers uniformly interspersed, as in Fig. 1(b). The number of weak scatterers N_w is fixed at 100, whereas the number of strong scatterers N_s and the ratio of the magnitudes of scattering amplitudes of the strong to the weak scatterers r_{sw} are both varied.

C. CF-Based Mixed Assemblage PDF Generation

As derived in Section II, the total echo pdf of a mixed assemblage can be obtained by evaluating the Bessel–Fourier series of the product of the CFs from the pdfs of an arbitrary number of arbitrary scatterers. By observing (14), it follows that the CF of the echo pdf of a single scatterer of each type [$\phi_m(\omega)$ in (14)] in the aggregation is necessary for calculating the echo pdf of mixed assemblages through (10). The echo pdf of a single weakest scatterer $p_A(a; N_1 = 1)$ is obtained by normalizing the echo pdf resulted from (11). The echo pdf $p_A(a; N_m = 1, r_m)$ is obtained by scaling $p_A(a; N_1 = 1)$ on the amplitude axis so that the ratio of the rms amplitude of the two echo pdfs equals to r_m. This operation is done by reversing the procedure of echo pdf normalization (Appendix B). The CFs of the echo pdfs can then be obtained through (8). As mentioned earlier (Section III-A), the echo pdf $p_S(s)$ of each scatterer before the beampattern effects is assumed to be Rayleigh distributed.

The CFs of the echo pdfs of the different types of scatterers calculated above can be multiplied according to (14) and converted using (10) to obtain the total mixed assemblage echo pdf. For the infinite series in (10), it was found that the contribution of the terms outside the range where ϕ^Σ reaches its first zero can be neglected due to the rapidly decreasing nature of ϕ^Σ and the associated Bessel functions. The higher the total energy in the echoes, i.e., the larger r_{sw} or N_s is, the more rapidly ϕ^Σ decreases. This can be intuitively understood by the time–frequency reciprocity of Fourier analysis.

The number of terms included in the evaluation of (10) is also determined by the value of $a_{\max}$, which controls the sampling resolution of ϕ^Σ. Although $a_{\max}$ is theoretically infinity in this study owing to the assumption of Rayleigh-distributed scatterers, approximating $a_{\max}$ to a moderate finite value can produce valid results, as will be shown in Section III-D. For mixed assemblages composed of two types of scatterers, this value can be chosen arbitrarily from the tail of the echo pdf of a single strong scatterer $p_A(a; N_s = 1; r_{sw})$ at an echo amplitude where the corresponding probability density is several orders of magnitude lower than the maxima of the echo pdf. Therefore, the larger r_{sw} is, the higher the value of $a_{\max}$, which conveniently corresponds to the need for a finer sampling of rapidly decreasing ϕ^Σ in these cases. This is conceptually analogous to the Nyquist sampling theorem in Fourier analysis. In this study, the value of $a_{\max}$ is adjusted according to the value of r_{sw} and generally falls in the range between several hundreds to lower thousands.

D. Validation of CF-Based Mixed Assemblage PDF (As a Predictor)

Theoretical predictions given by the CF-based mixed assemblage pdf are validated by numerical simulations generated over a wide range of ratios of the magnitudes of scattering amplitudes. The investigated cases include mixed assemblages composed of two and three types of scatterers with the number of scatterers varying from 1 to 100 and the ratios of the magnitudes of scatterer amplitudes varying from 2 to 60, both with an increment of 1.

The theoretical CF-based mixed assemblage pdf and the simulated data agree well in all investigated cases. However, only a representative subset of the model validation results from mixed assemblages consisting of two types of scatterers are shown here to avoid excessive repetition (Fig. 2). One set of echo pdfs with a small value of r_{sw} $(= 5)$ and another set of echo pdfs with a larger value of r_{sw} $(= 20)$ are selected. The values of N_s $(= 1, 10, 50)$ are selected based on the observation that the shape of the echo pdfs asymptotically approaches the Rayleigh distribution with increasing N_s (see Section III-E).

It is found that the accuracy of the predicted mixed assemblage pdfs is related to the accuracy of the echo pdf of a single weakest scatterer $p_A(a; N_1 = 1)$, which is the most basic component in generating the CF-based mixed assemblage pdfs (see Section III-C). Despite the generally good agreement between the theoretical pdf curves and the simulated data (Fig. 2), minor deviations are observed in both the echo pdf tail and the region where the echo amplitudes are low and probability densities are high (referred to as the "low-amplitude region" below and indicated by an arrow in Fig. 2). These small deviations are jointly caused by inaccuracies in the unnormalized model predictions and the normalization procedure. Specifically, inaccuracies in $p_A(a; N_1 = 1)$ result in inaccuracies in the low-amplitude region of unnormalized theoretical pdf curves. The energy contained in this region affects the rms echo amplitude used for normalization (see Appendix B) which, in turn, results in deviations in both the tail and the low-amplitude region of the normalized echo pdf models. This problem can be serious for echo pdfs associated with using beampatterns with many sidelobes, such as in the cases when ka_T is large. This is because echoes in the low-amplitude region are primarily contributed by measurements from the sidelobes. These inaccuracies are due to numerical issues associated with small numbers.

E. Effect of Mixed Assemblage Composition on the Echo PDF

The effects of mixed assemblage composition on the shape of the echo pdfs are examined in cases consisting of only two types of scatterers.

1) Varying the Ratio of Scattering Amplitudes: The shape of the echo pdf is shown to change by varying r_{sw} while keeping N_s and N_w fixed (Fig. 3). When r_{sw} is small (top panels), the echo contributions from the strong scatterers are more confined to the tail of the pdfs. The lower amplitude portion of the pdfs, which is dominated by the weak scatterers, remains relatively stable. However, when r_{sw} is increased (bottom panels), the scattered field is increasingly dominated by the strong scatterers, and the energy contained in the tail of the pdfs is of a higher proportion of the total scattered energy. Therefore, in addition to an elevated heavy tail, the modes of the normalized pdfs with larger r_{sw} are displaced toward smaller echo amplitudes.

2) Varying the Number of Scatterers in Each Type: The shape of the echo pdf also varies with changing N_w and N_s while holding r_{sw} fixed (Fig. 3). When N_s is small, the curves are highly non-Rayleigh owing to occasional large echoes from the strong scatterers occurring in the mainlobe of the beam. As N_s increases, the shape of the echo pdf gradually approaches the Rayleigh distribution. This trend of variation from non-Rayleigh toward the Rayleigh distribution with increasing number of scatterers is the same as the results reported in [8] for assemblages consisting of only one type of scatterer. This property has an impact on the use of echo pdfs to infer the composition of mixed assemblages, as will be discussed in Section IV-D. Furthermore, as N_s increases, the total scattered field is increasingly dominated by the strong scatterers, and the contribution from the weak scatterers becomes negligible. This explains why echo pdfs with the combination $(N_s = 0, N_w = 100)$ and $(N_s = 100, N_w = 100)$ are almost identical, regardless of the value of r_{sw}.

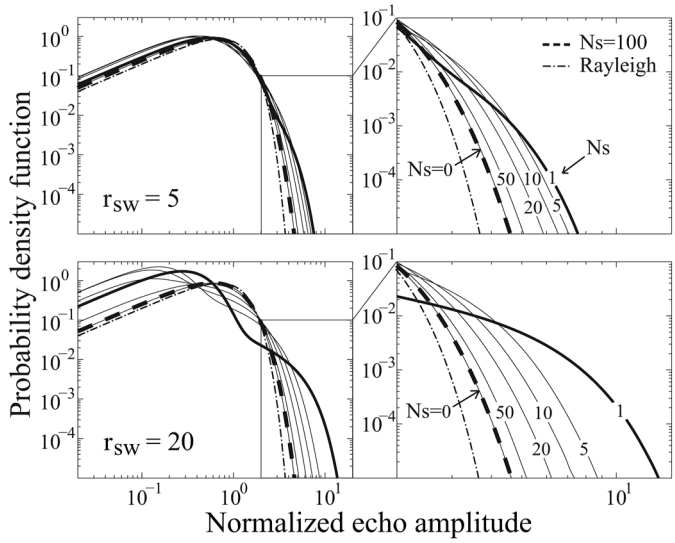

Fig. 3. Variation of the CF-based mixed assemblage pdf as a function of mixed assemblage composition. The top and bottom plots show the effects of changing $N_s(= 0, 1, 5, 10, 20, 100)$ on the shape of the echo pdf when $r_{sw} = 5$ and $r_{sw} = 20$, respectively. N_w is fixed at 100 in all plots. Note that the $N_s = 0$ and $N_s = 100$ curves are nearly identical as explained in the text.

IV. Comparison of the CF-Based Mixed Assemblage PDF and M-Component Mixture Model

In this section, the performance of the newly developed CF-based mixed assemblage pdf is compared with the commonly used M-component mixture model in their use to infer parameters of simulated mixed assemblages [Fig. 1(b)] and split aggregations [Fig. 1(a)]. The goal of this analysis is to investigate the impact of the mismatch between model assumptions and the actual scattering processes on echo interpretation. The simulated data are fit to model pdfs with varying parameters through a best-fit procedure involving MLEs. The parameters of the aggregation composition corresponding to the best-fitting pdfs (i.e., the inferred parameters) are then compared with the true parameters used in numerical simulations. The discrepancies between the true and inferred parameters given by each model are compared. To simplify the analysis, the number of scatterer types is limited to two $(M = 2)$ for all calculations as in the earlier examples.

A. Generation of Simulated Mixed Assemblages and Split Aggregations

Echo pdfs of both simulated mixed assemblages and split aggregations are obtained by forming the number frequency histograms of ensembles of normalized simulated realizations (see Section III-A and Appendix B for details of normalization). The ensembles are formed differently in these two cases depending on the spatial arrangement of the different types of scatterers in the analysis window.

For mixed assemblages, each independent realization is generated by coherently summing the contribution from both the strong and weak scatterers according to the procedure described in Section III-B. Therefore, all simulated realizations in an ensemble are drawn from the same scattering process. Recall that the strong and weak scatterers are uniformly dispersed within an analysis window in mixed assemblages [Section I, Fig. 1(b)].

For split aggregations, each independent realization is formed by summing the contribution from either only the strong or only the weak scatterers. Therefore, any given ensemble would contain two subsets of realizations drawn from two independent scattering processes: one consists of N_s strong scatterers, and the other consists of N_w weak scatterers. This reflects the spatial segregation of the two types of scatterers within the analysis window [Section I, Fig. 1(a)]. For all simulated split aggregations in this study, the proportions of realizations drawn from the strong and weak scatterer subsets are fixed at 0.05 and 0.95, respectively. In other words, of a total of 10^4 realizations in one ensemble, 500 and 9500 realizations are drawn from the processes involving the strong and weak scatterers, respectively.

In this study, the number of weak scatterers N_w is fixed at 100 for all cases, whereas the number of strong scatterers N_s is varied through the following values: 1, 2, 5, 10, 20, 50, and 100. The ratio of the magnitudes of scattering amplitudes of the strong to weak scatterers r_{sw} is varied through the following values: 5, 10, 15, 20, 30, and 40. These parameter values are chosen based on: 1) the understanding that important scattering scenarios in nature often involve a background of numerous weak scatterers and only a few strong scatterers (Section I); and 2) the observation that the shape of an echo pdf approaches the Rayleigh distribution asymptotically with increasing N_s (Section III-E).

All simulated data sets shown in this paper contain 10^4 independent realizations. For both mixed assemblages and split aggregations, inference analysis is conducted for 20 sets of simulated data for each parameter combination. The statistics of the inferred parameters are reported (Section IV-D). Simulated data sets containing 10^3 independent realizations were also generated and analyzed to provide a reference for the model performance in potential field conditions where the number of echo samples is limited. Due to the focus of this parameter inference study on the impact of mismatches between model assumptions and the actual scattering processes, these additional results are only briefly discussed on their implication in the analysis of field data.

B. Echo Statistic Models Formulated for Two Types of Scatterers

Using the general formulations (1) and (3) in Section I, the CF-based mixed assemblage pdf and the M-component mixture model are given here in simplified forms for the case of only two types of scatterers. From (3), the CF-based mixed assemblage pdf for two types of scatterers is

$$p_A^{\Sigma}(a)_{,\,\text{CF-based}} = p_A^{\Sigma}(a; N_w, N_s, r_{sw}). \tag{17}$$

From (1), the two-component mixture model is

$$p_A^{\Sigma}(a)_{,\,\text{mixture}} = (1 - w_s)p_{A,w}(a) + w_s p_{A,s}(a) \tag{18}$$

where $p_{A,w}(a)$ and $p_{A,s}(a)$ are the component pdf for the weak and strong scatterers, respectively, and w_s is the proportion of strong scatterers in the echo samples.

As with the more general (1) and (3), (17) is from a coherent summation of the contribution from both strong and weak scatterers, whereas (18) considers the total echo distribution as a sum of two independent scattering processes, with each sample drawn from either of the two processes.

Two versions of the two-component mixture model are used in this model comparison study. In the first version, the component pdfs are two Rayleigh distributions with different magnitudes of the scattering amplitudes related by a ratio of r_{sw}, i.e.,

$$p_{A,w}(a) = p_{A,\text{Rayleigh}}(a; 1) \text{ and } p_{A,s}(a) = p_{A,\text{Rayleigh}}(a; r_{sw}). \tag{19}$$

The use of a Rayleigh distribution implies that each echo sample is from a large number of unresolvable scatterers filling the beam, i.e., $N_w \to \infty$ and $N_s \to \infty$. This version of the two-component mixture model will be referred to as the "two-component Rayleigh mixture model."

In the second version, the component pdfs are calculated using the CF-based echo pdf formulation, but with only one type of scatterer in each component. Specifically, $p_{A,w}(a)$ and $p_{A,s}(a)$ are calculated using (10) and

$$\phi_w^{\Sigma} = (\phi_w(\omega))^{N_w} \quad \text{and} \quad \phi_s^{\Sigma} = (\phi_s(\omega))^{N_s}. \tag{20}$$

The magnitudes of the scattering amplitudes of these two types of scatterers are also related by a ratio of r_{sw}. This version of the two-component mixture model will be referred to as the "two-component CF-based mixture model."

Note that in the context of simulated mixed assemblages where the different types of scatterers are uniformly interspersed [Fig. 1(b)], the proportional factor w_s in the above two mixture models does not have a physical meaning. Similarly, this factor is not included in the formulation of the CF-based mixed assemblage pdf when this model is applied to analyze simulated split aggregations [Fig. 1(a)]. These differences in model parameterization have impacts on the results of inference, which will be discussed in Section IV-D.

Furthermore, for completeness, the candidate model sets for both the CF-based mixed assemblage pdf and the two-component CF-based mixture model include the cases in which there is only one type of scatterer in the analysis window (referred to as the "monotype aggregation"). The echo pdf of monotype aggregations can be described using the CF-based echo pdf formulation with only one type of scatterer in the analysis window [8]. This model will be referred to as the "one-component CF-based echo pdf," which can be obtained using the combination of (10) and (20), with N_w set to 0. Examples of the one-component CF-based echo pdf can be seen in Appendix B. The candidate model set for the two-component Rayleigh mixture model also includes the case where there is only one Rayleigh-distributed component.

C. Method of Parameter Inference

The composition of each simulated mixed assemblage or split aggregation is inferred by fitting the echo pdf models described in Section IV-B to the simulated data. Parameters of the best-fitting model pdf are taken as the inferred parameters of the mixed assemblage or split aggregation composition. The MLE [30] is

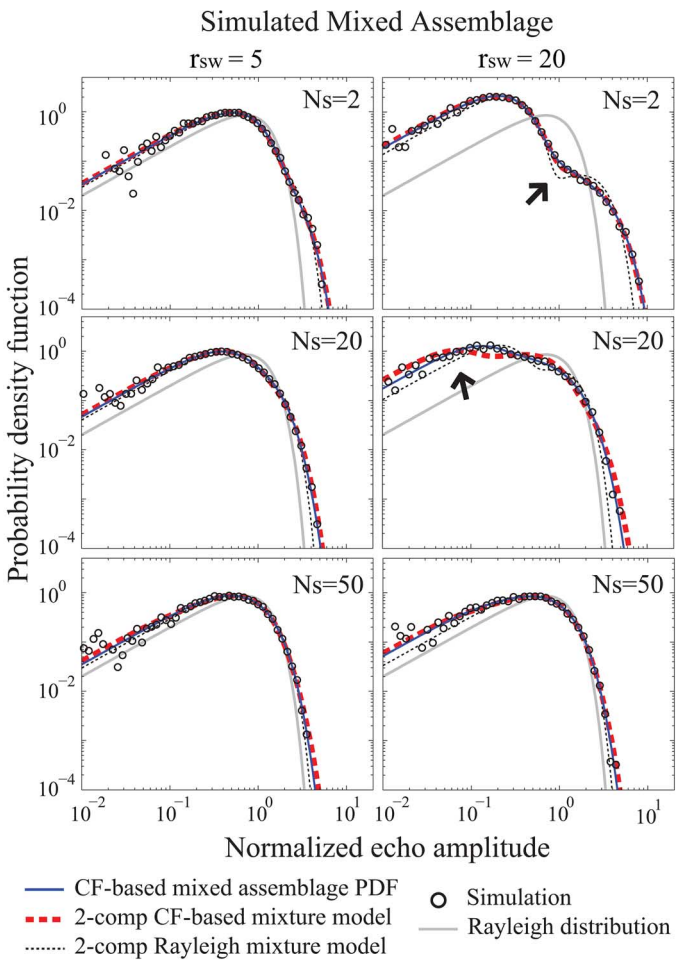

Fig. 4. Several representative examples of the echo pdf of simulated mixed assemblages composed of two types of scatterers (◯) and their corresponding best-fitting echo pdf models (lines). Also shown on the plots are the true values of r_{sw} and N_s used to generate the simulated data. The true value of N_w is fixed at 100 for all cases. The best-fitting parameters for each of the models are summarized in Fig. 6. The arrows indicate the locations where the best-fitting mixture models have noticeable deviation from the data.

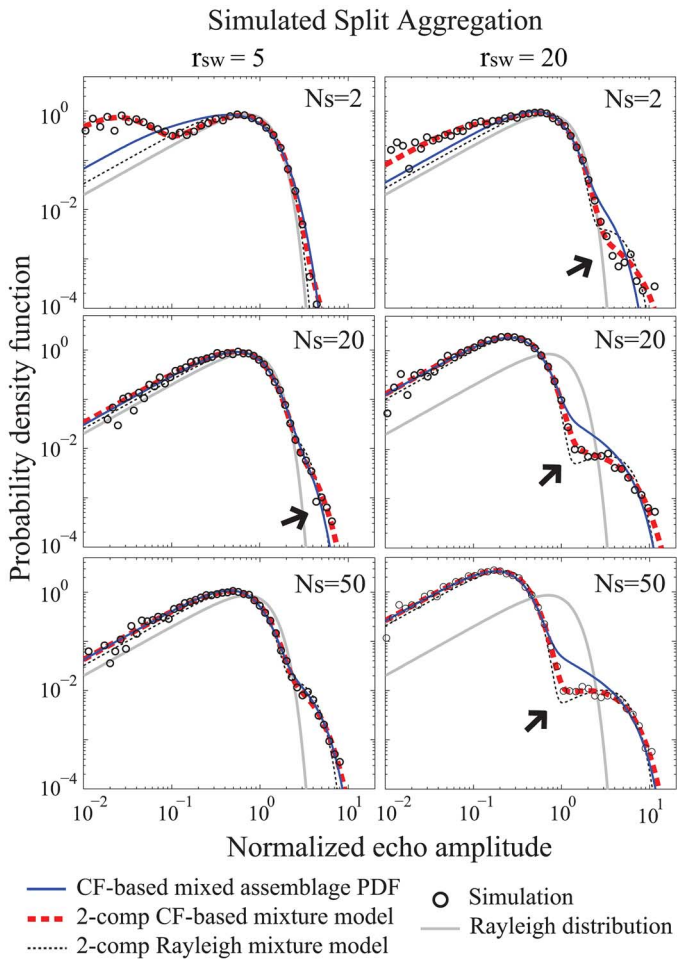

Fig. 5. Several representative examples of the echo pdf of simulated split aggregations composed of two types of scatterers (◯) and their corresponding best-fitting echo pdf models (lines). Also shown on the plots are the true values of r_{sw} and N_s used to generate the simulated data. The true value of N_w is fixed at 100 for all cases. The best-fitting parameters for each of the models are summarized in Fig. 7. Note the best-fitting CF-based mixed assemblage pdf in the case with true $r_{sw} = 5$ and true $N_s = 2$ fails to achieve a better fit than the one-component CF-based echo pdf. Therefore, the best-fitting one-component CF-based echo pdf is displayed here. The arrows indicate the locations where the best-fitting CF-based mixed assemblage pdfs have noticeable deviation from the data.

used in the best-fit procedure. Assume $x_1, x_2, \ldots, x_n$ constitute an ensemble of simulated independent and identically distributed echo samples, the MLE computes the log-likelihood

$$\begin{aligned} l(\boldsymbol{\rho}|x_1, x_2, \ldots, x_n) &= \ln p_{\text{model}}(x_1, x_2, \ldots, x_n|\boldsymbol{\rho}) \\ &= \ln \prod_i^n p_{\text{model}}(x_i|\boldsymbol{\rho}) \\ &= \sum_i^n \ln p_{\text{model}}(x_i|\boldsymbol{\rho}) \end{aligned} \tag{21}$$

and performs the inference by maximizing the log-likelihood

$$\hat{\boldsymbol{\rho}}_{\text{MLE}} = \arg\max_{\boldsymbol{\rho}} l(\boldsymbol{\rho}|x_1, x_2, \ldots, x_n) \tag{22}$$

where $\boldsymbol{\rho} = \{N_w, N_s, r_{sw}\}$ for the CF-based mixed assemblage pdf, $\boldsymbol{\rho} = \{N_w, N_s, r_{sw}, w_s\}$ for the two-component CF-based mixture model, and $\boldsymbol{\rho} = \{r_{sw}, w_s\}$ for the two-component Rayleigh mixture model. In this study, the parameter space of N_s spans from 1 to 100 with an increment of 1. The parameter space of r_{sw} spans from 2 to 60 with an increment of 1. The parameter space of w_s spans from 0.01 to 0.5 with an increment of 0.01. The value of N_w is fixed at 100. For the one-component CF-based echo pdf, the parameter space of the number of scatterers in monotype aggregations spans from 1 to 100 with an increment of 1.

The goodness of fit of the best-fitting echo pdf models is evaluated using the asymptotic p-values associated with the Kolmogorov–Smirnov (KS) test [31] and the upper-tailed Anderson–Darling (AD) test [32]. The KS test statistic is generally used to quantify the overall measure of fit of the pdf model, whereas the upper-tailed AD test places more weight on observations in the tail of the distribution [32]. The p-value is a nonlinear, one-to-one mapping that transforms the test statistics to the scale of (0, 1) that represents the probability that the simulated data are drawn from the distribution given by the best-fitting echo pdf model. Note that because the model parameters are inferred, these values should not be interpreted as accurate p-values; rather, these approximate p-values should

TABLE I
GOODNESS OF FIT OF THE BEST-FITTING ECHO PDF MODELS MEASURED USING APPROXIMATE p-VALUES ASSOCIATED WITH THE KS TEST AND THE UPPER-TAILED AD TEST. THE VALUES INCREASE TOWARD ONE AS THE FIT IMPROVES. THE HIGHEST VALUE FOR EACH PARAMETER COMBINATION OF SIMULATED DATA (EACH ROW) IS SHOWN IN BOLD. NOTE THE BEST-FITTING CF-BASED MIXED ASSEMBLAGE PDF IN THE SIMULATED SPLIT AGGREGATION WITH TRUE $r_{sw} = 5$ AND TRUE $N_s = 2$ FAILS TO ACHIEVE A BETTER FIT THAN THE ONE-COMPONENT CF-BASED ECHO PDF. THEREFORE, THE MEASURE OF FIT OF THE BEST-FITTING ONE-COMPONENT CF-BASED ECHO PDF FOR THIS CASE IS SHOWN HERE (SPECIFICALLY INDICATED BY "$*$")

			Simulated mixed assemblage			**Simulated split aggregation**		
	r_{sw}	N_s	CF-based mixed assemblage PDF	2-comp CF-based mixture model	2-comp Rayleigh mixture model	CF-based mixed assemblage PDF	2-comp CF-based mixture model	2-comp Rayleigh mixture model
KS	5	2	0.0129	**0.6275**	3.88×10^{-5}	5.24×10^{-18} ($*$)	**0.6611**	6.07×10^{-10}
		20	**0.7057**	0.0125	0.0095	0.0448	**0.3609**	2.00×10^{-9}
		50	**0.8025**	0.2962	0.0139	0.0034	**0.6976**	1.49×10^{-10}
	20	2	0.2535	**0.7314**	5.68×10^{-18}	4.25×10^{-7}	**0.7743**	7.57×10^{-28}
		20	**0.4846**	3.83×10^{-6}	6.93×10^{-22}	3.37×10^{-3}	**0.6757**	2.27×10^{-20}
		50	**0.8258**	0.2889	0.0016	1.73×10^{-15}	**0.4557**	4.12×10^{-20}
AD	5	2	0.0488	**0.9333**	8.38×10^{-4}	2.19×10^{-5}	**0.6272**	0.0019
		20	**0.9080**	0.0058	0.0025	0.0201	**0.4426**	3.97×10^{-6}
		50	**0.8669**	0.2184	0.0429	0.0034	**0.7233**	4.68×10^{-8}
	20	2	0.4362	**0.7112**	3.35×10^{-12}	2.38×10^{-5}	**0.9049**	6.82×10^{-20}
		20	**0.4927**	2.04×10^{-14}	2.40×10^{-17}	9.56×10^{-21}	**0.7853**	5.78×10^{-14}
		50	**0.8520**	0.2042	0.0359	4.60×10^{-17}	**0.7853**	2.36×10^{-12}

be treated as measures of fit where the best fit is achieved as the measure approaches one [13].

D. Performance of Models as Inference Tools

In this section, the performances of the CF-based mixed assemblage pdf and the two two-component mixture models in their use as inference tools are evaluated. The evaluation is based on the fit of the shape of the echo pdfs (Figs. 4 and 5, and Table I) and the accuracy of inferred parameters of the composition of simulated mixed assemblages or split aggregations (Figs. 6 and 7).

1) Fit of the Shape of Echo PDFs: For simulated mixed assemblages, both the CF-based mixed assemblage pdf and the two-component CF-based mixture model are capable of successfully fitting the shape of the echo pdf of simulated data for most investigated cases (Fig. 4). Detailed inspection of the fitting results reveals that the best-fitting two-component CF-based mixture model sometimes shows small deviation from the simulated data near the "inflection points" of the echo pdfs or in the low-amplitude region (indicated by arrows in Fig. 4). The two-component Rayleigh mixture model generally fails to produce an appropriate fit of the shape to the simulated data in all cases, most notably on the levels near the inflection points (also indicated by the arrows) and the slope of the tails. The above observations are generally reflected in the measures of fit associated with the KS test and the upper-tailed AD test (Table I). The best-fitting model varies between the CF-based mixed assemblage pdf and the two-component CF-based mixture model depending on the composition of the simulated assemblage. The two-component Rayleigh mixture model fits the worst in all cases.

For simulated split aggregations, only the two-component CF-based mixture model is capable of producing satisfactory fit to the shape of the echo pdfs of simulated data (Fig. 5). The CF-based mixed assemblage pdf generally fails to fit the simulated split aggregations in most investigated cases. The deviation is particularly large at the inflection points or at the tails of the echo pdfs (indicated by arrows in Fig. 5). Furthermore, in cases when both the true N_s and r_{sw} are small (e.g., $N_s = 2$ and $r_{sw} = 5$), the CF-based mixed assemblage pdf also fails to provide a better fit than the one-component CF-based echo pdf for all 20 simulated data sets (Fig. 7). Therefore, the best-fitting one-component echo pdf is shown for this case in Fig. 5. The fit only improves in the tail when N_s is large (e.g., $N_s = 50$). Similar to the results in the case of simulated mixed assemblages, the two-component Rayleigh mixture model also fails to produce appropriate fit to the shape of the echo pdf of simulated split aggregations in all investigated cases, most notably on the level near the inflection points and the slope of the tails. The measures of fit using KS statistics and upper-tailed AD statistics generally correspond with the above observations (Table I). The two-component CF-based mixture model gives the best fit to the simulated data in all cases.

The above observation on the fit (or lack of fit) of the shape of echo pdf models to simulated data can be explained based on the validity of model assumptions in each case and the number of free parameters in the model formulation. First, the two-component Rayleigh mixture model fails in all investigated cases due to its erroneous assumption on the presence of an infinite number of scatterers in the sonar/radar beam. By rigorously incorporating the beampattern effects (see Section I), the CF-based mixed assemblage pdf and the two-component CF-based mixture model are more likely to produce satisfactory fit to the shape of the echo pdfs of simulated data.

The two-component CF-based mixture model is more versatile than the CF-based mixed assemblage pdf when the fit of the shape of echo pdfs is considered. In particular, the slope and level (i.e., probability density) of the tail of the CF-based

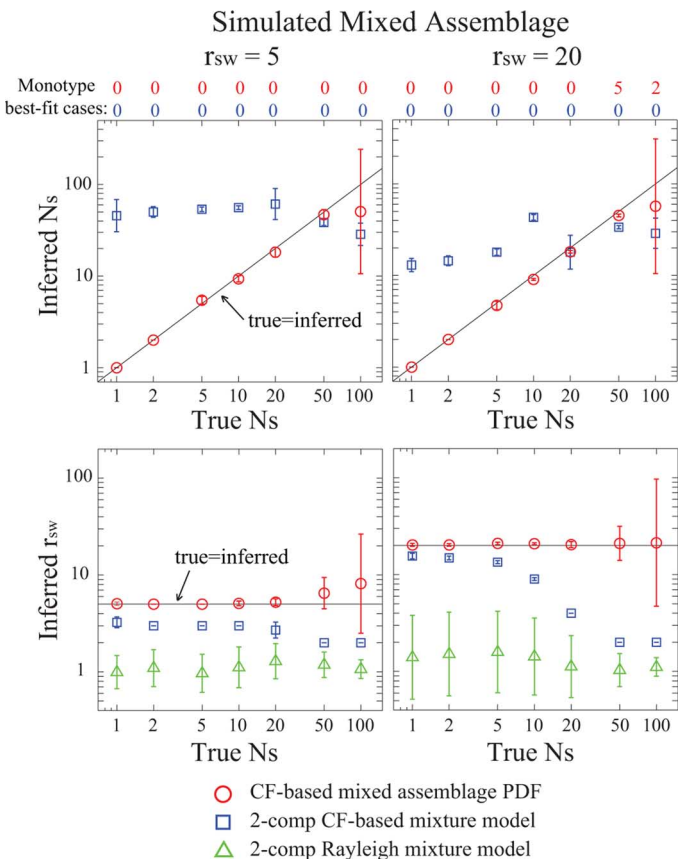

Fig. 6. Comparison of the best-fitting inferred model parameters versus the true parameters for simulated mixed assemblages composed of two types of scatterers. The inferred parameters vary as functions of the true values of N_s in the simulation and the type of model. The symbols and errorbars represent the mean and standard deviation calculated using the inferred parameters from 20 sets of simulated mixed assemblages. Inferred parameters from cases where the simulated data are best-fitted by the one-component CF-based echo pdfs are discarded. The numbers of discarded cases in fitting the CF-based mixed assemblage PDF and the two-component CF-based mixture model are listed on top of the figures in the first and second rows, respectively. Due to differences in model parameterization, only the inferred r_{sw}'s are reported for the two-component Rayleigh mixture model.

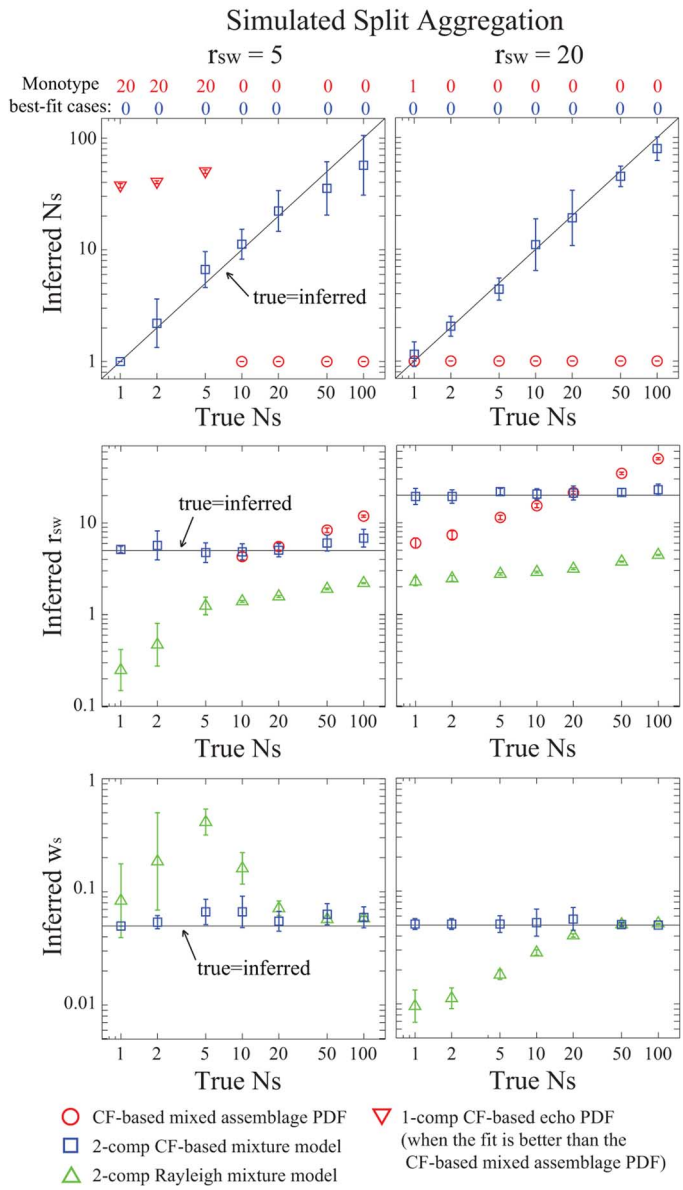

Fig. 7. Comparison of the best-fitting inferred model parameters versus the true parameters for simulated split aggregations composed of two types of scatterers. The inferred parameters vary as functions of the true values of N_s in the simulation and the type of model. The symbols and errorbars represent the mean and standard deviation calculated using the best-fitting inferred parameters of 20 sets of simulated split aggregations. Details of the calculation of the mean and standard deviation are described in the caption of Fig. 6. The symbol for the CF-based mixed assemblage pdf is changed from ◯ to ▽ when the best-fitting CF-based mixed assemblage pdf fails to achieve a better fit than the one-component CF-based echo pdf in all 20 sets of simulated data of a particular composition of split aggregation. This includes the cases with true $r_{sw} = 5$ and true $N_s = 1, 2, 5$. The symbol ▽ in these cases represents the mean of the number of scatterers in the one-component CF-based echo pdf. Due to differences in model parameterization, N_s does not exist for the two-component Rayleigh mixture model, and w_s does not exist for the CF-based mixed assemblage pdf.

mixed assemblage pdf are inherently linked through model parameters N_w and N_s, and the associated beampattern effects [7], [8]. These physics-based properties therefore limit the general shape-fitting flexibility of this model. In contrast, although the slope of the tail of the two-component CF-based mixture model is similarly determined by N_s and the beampattern effects, the level of the tail can be adjusted freely through the additional proportional parameter w_s in (18). This makes the two-component CF-based mixture model more flexible in fitting the shape of the echo pdfs.

In the Rayleigh mixture case, it is likely that the fit of the shape of echo pdfs can be improved by using more than two components in the mixture model through (1) [16]. However, with simulated data generated from only two types of scatterers, any extra components would lack physical meanings and do not connect with the underlying scattering processes.

2) Accuracy of the Inferred Parameters: The inferred composition of simulated mixed assemblages and split aggregations with several representative combinations of true N_s and r_{sw} are illustrated (Figs. 6 and 7). The mean and standard deviation of the inferred parameters are calculated by compiling the best-fitting results from 20 sets of simulated data for each combination of parameters. Note that the inferred parameters from the cases where the simulated data are best-fitted by the one-component CF-based echo pdf are discarded, except for the cases when all 20 sets of simulated data with the same composition are best-fitted by the one-component CF-based echo pdf. In

such cases, the mean and standard deviation of the best-fitting number of scatterers are calculated and reported. The inferred w_s is only meaningful in the context of simulated split aggregations, as discussed in Sections I and IV-B.

For simulated mixed assemblages, only the CF-based mixed assemblage pdf can accurately infer the values of N_s and r_{sw} (Fig. 6). Furthermore, the accuracy of this pdf is limited to a subset of the conditions explored. The inferred parameters are the most accurate when the true N_s is small. The model performance degrades in a form of increasing standard deviation with increasing N_s. This can be explained by the fact that variation in the shape of the CF-based mixed assemblage pdf is inherently small when N_s is large and the pdf correspondingly approaches the Rayleigh distribution (Section III-E). The two-component CF-based mixture model overestimates N_s except for in the cases when true N_s is large. This model also underestimates r_{sw} in all investigated cases. The two-component Rayleigh mixture model underestimates r_{sw} in all investigated cases.

For simulated split aggregations, only the two-component CF-based mixture model is capable of accurately inferring the values of N_s, r_{sw}, and w_s (Fig. 7). When both the true r_{sw} and N_s are small ($r_{sw} = 5$ and $N_s = 1, 2, 5$), the CF-based mixed assemblage pdf fails to achieve a better fit than the one-component CF-based echo pdf for all 20 sets of simulated data with the same composition. In other cases, the CF-based mixed assemblage pdf underestimates N_s and either underestimates or overestimates r_{sw}, depending on the composition of the simulated split aggregations. The two-component Rayleigh mixture model underestimates r_{sw} in all investigated cases, and either overestimates or underestimates w_s, depending on the true N_s and r_{sw}.

Note the discussion here on the inference accuracy only considers the best inferred parameters without referencing to the fit of the shape of echo pdfs. This is done with an aim to demonstrate the impact of the mismatch between model assumptions and the actual scattering processes on the accuracy of the inferred parameters. In practice, adequate fit on the shape of echo pdfs should be simultaneously considered for valid interpretation of field data.

Furthermore, only the results of parameter inference using data sets consisting of 10^4 independent realizations are presented in this section. The results obtained using data sets consisting of 10^3 independent realizations are similar to those shown in Figs. 6 and 7. However, standard deviations of the inferred parameters in these cases are generally larger, especially in the cases where N_s is small and the tail of the echo pdf is heavy (Section III-E). This is likely caused by insufficient sampling in the tail region when the total number of samples is small. This suggests that statistical analysis of field data should be treated with caution when the number of observation samples is limited. A more thorough study on the accuracy and variation of parameter estimates as a function of sample number using simulated data or resampled field measurements is needed to fully characterize this relationship.

3) Summary and Discussion: Results of this parameter inference study using simulated data show the following. 1) Although each type of model pdf can be made to fit the simulated data in some conditions, the accuracy of the inferred parameters varies dramatically, depending on whether the model assumptions match with the actual physical scattering processes of the simulated scenario. 2) The two-component CF-based mixture model can produce adequate fit to the shape of the echo pdfs of most simulated data sets, regardless of the physical scattering processes. This is a direct consequence of the inclusion of the proportional parameter, w_s, in the model formulation of (18). However, the inferred parameters are only accurate and meaningful when the data are generated from split aggregations. 3) The CF-based mixed assemblage pdf can only produce accurate inferred parameters and adequate fit to the shape of echo pdfs for data generated from mixed assemblages. This limitation results directly from the physics-based properties of this model, through which the slope and level of the tail of the echo pdfs are inherently determined by the number of the different types of scatterers in the sonar/radar beam and the associated beampattern effects. Furthermore, the inferred parameters are only meaningful for simulated mixed assemblages. 4) The two-component Rayleigh mixture model generally fails to fit the shape of the echo pdf of all simulated data, because the Rayleigh distribution is not adequate for describing the scattering from a finite number of scatterers with associated beampattern effects.

It should be noted that although the above analysis is based on normalized echo pdfs, in practice, the absolute scattering levels in unnormalized echo pdfs may provide important information for identifying scatterers and should be considered in the analysis. In addition, both the simulated data and the models are "noise free." The influence of ambient noise and system noise should be incorporated in the models for the analysis of real-world data [24].

Furthermore, the simulated data here are generated under idealized scenarios where both the number of scatterer types and the number of scatterers of each type within an analysis window are deterministic, rather than random. In reality, these parameters of aggregation composition can change on a ping-by-ping basis and may be more properly modeled as random variables in a Bayesian framework. In the case of split aggregations, echo samples may also be collected at the interface between different types of scatterers where more than one type of scatterer is included in the resolution cell. The scattering processes in these cases are similar to those in mixed assemblages, rather than split aggregations. The impacts of these interface samples may be negligible if the total echo ensemble is large. A simulation study that incorporates the actual system parameters and experimental conditions is needed to address this question.

Finally, although the mixture models and the CF-based mixed assemblage pdf are considered separately in this study, an overarching mixture model with all the models considered here as component pdfs can be useful in the representation and analysis of the statistics of real-world echoes collected in many different environments using different systems.

V. Summary and Conclusion

In this paper, a general expression for the echo pdf of mixed assemblages is formulated based on the method of CFs. By incorporating the beampattern effects from an axisymmetric transceiver aperture, the theoretical pdf curves are validated by numerical simulations and shown to have high accuracy over a

wide range of conditions. The CF-based mixed assemblage pdf is observed to be highly non-Rayleigh when the number of the strongest type of scatterer in the assemblage is low and gradually approaches the Rayleigh distribution as the number of the strongest type of scatterer increases.

This new CF-based mixed assemblage pdf significantly outperforms the commonly used M-component mixture model (Rayleigh-based and CF-based) when used as a tool to infer the parameters of simulated mixed assemblages composed of two types of scatterers. The two-component Rayleigh mixture model generally fails to adequately fit the shape of the echo pdf of simulated data. The two-component Rayleigh-based mixture model and the two-component CF-based mixture model also both result in up to order-of-magnitude errors in the parameter estimates. In spite of the high accuracy in predicting the echo statistics from mixed assemblages, the usefulness of the CF-based mixed assemblage pdf in inferring the assemblage composition from simulated data is limited to cases where the number of dominant scatterers is relatively small. This is because changes in the shape of these pdfs owing to changes in the number of scatterers are inherently small when the number of scatterers is large.

However, when split aggregations composed of two types of scatterers are considered, the CF-based mixed assemblage pdf generally fails to adequately fit the shape of the echo pdf of simulated data and also produces up to order-of-magnitude errors in the parameter estimates. The two-component Rayleigh mixture model also generally fails to fit the shape of the echo pdf of simulated data, whereas the two-component CF-based mixture model outperforms the other models in both the fit of the shape of echo pdfs and the accuracy of parameter estimates. The CF-based mixed assemblage pdf is limited in its flexibility to fit the shape of echo pdfs due to its physics-based properties. Specifically, the shape of this echo pdf model is inherently determined by the number of scatterers in the sonar/radar beam and the associated beampattern effects (Section I, [7], [8]). In contrast, the shape of the two-component CF-based mixture model is more flexible owing to the additional proportional parameter in the model formulation.

The results show that, to accurately model and analyze the echo statistics of aggregations composed of more than one type of scatterer (either mixed assemblages or split aggregations), it is important to: 1) rigorously account for the scattering from a finite number of scatterers and the associated beampattern effects; and 2) rigorously account for the spatial distribution of the different types of scatterers when combining their scattering contribution to the echo. Even though any given model may be made to fit the echo pdf of data in some conditions, mismatches between model assumptions and the actual scatterer distribution can lead to order-of-magnitude errors in data interpretation. Although only two relatively simple mixture models (CF-based and Rayleigh-based) are investigated along with the new CF-based mixed assemblage pdf in this study, the above conclusions are important and applicable to the general analysis of echo statistics.

Finally, it is important to note that all results involve N, the number of scatterers in the *half-space*. As discussed above, once weighted by the beampattern, the *effective* number of scatterers, that is, the number approximately within the resolution cell, will be much smaller.

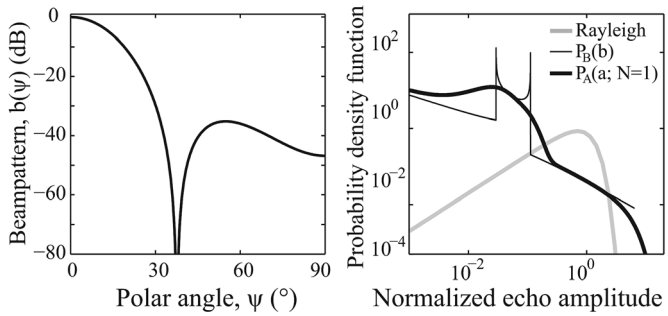

Fig. 8. Beampattern $b(\psi)$, beampattern pdf $p_B(b)$, and the associated echo pdf with only one scatterer in the sonar/radar beam $p_A(a; N = 1)$. The transceiver aperture is circular and asymmetric with $ka_T = 2\pi$ as in (13).

This study is inspired in the context of acoustic studies of mixed biological aggregations in the ocean, and the examples given in this paper are specific to volume backscattering sources with an axisymmetric transceiver aperture. However, the formulation of the CF-based mixed assemblage pdf is applicable to other types of mixed assemblages in different environments measured with different systems. This new predictive physics-based model can be used to synthesize potential measurements under a given scattering environment, which can aid in the design of experiments and provide information toward classifying and discriminating between various kinds of aggregations in nature through use of sonar/radar systems.

Appendix A
Beampattern, Beampattern PDF, and Associated Echo PDFs

This section provides details of the numerical evaluation of the beampattern, beampattern pdf, and associated echo pdfs discussed in Section II-C. The beampattern $b(\psi)$ of an asymmetric circular transceiver aperture with $ka_T = 2\pi$ is evaluated numerically through (13) [Fig. 8(a)]. The corresponding beampattern pdf $p_B(b)$ is evaluated numerically through (12) using finite difference with a step size of $10^{-4}\pi$ [Fig. 8(b)]. The step size determines the smallest echo amplitude (the leftmost point on the pdf) and the height of the discontinuities in the resultant beampattern pdf [the "spikes" in Fig. 8(b)]. For a single scatterer randomly located in the sonar/radar beam, the echoes "seen" through the system are modified by the beampattern effects (Section I). The resultant echo pdf $p_A(a; N = 1)$ can be evaluated numerically through (11) [Fig. 8(b)]. Here, the echo pdf $p_S(s)$ before the beampattern effects is assumed to be Rayleigh distributed, given by (16). A logarithmically spaced vector spanning a finite range (from 10^{-4} to 50 with 1000 logarithmically spaced points) is used to prescribe the points at which $p_S(s)$ and $p_A(a; N = 1)$ are calculated. Therefore, the largest element in this vector determines the upper limit of the numerical integration in (11). Although the Rayleigh distribution starts at zero and extends toward infinity on the amplitude axis, the range spanned by this vector is found sufficient for validating the CF-based mixed assemblage echo pdf model developed in this study.

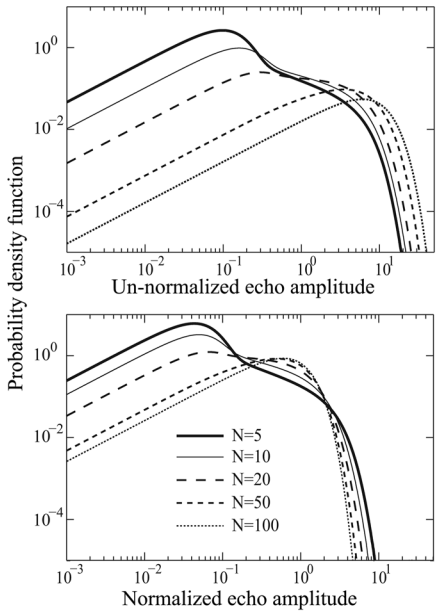

Fig. 9. Comparison of several original unnormalized (top) and normalized (bottom) one-component CF-based echo pdfs with varying numbers of only one type of scatterer (N).

Appendix B
Normalization of Echo PDFs

As discussed in Section III, the normalization procedure removes the echo pdfs' dependency on the absolute scattering amplitudes of the scatterers and other environment- and system-specific parameters, such as range-dependent transmission loss and system gain. This enables direct analysis of the aggregation composition using a set of standard normalized curves. For a set of discrete echo samples, the echo amplitude of each sample is normalized by the rms amplitude of all samples, which is calculated by

$$A_{\mathrm{rms}} = \sqrt{\sum \frac{x_q^2}{N}} \tag{23}$$

where x_q denotes the qth sample out of a total of N samples. For a given pdf $p_X(x)$, each point on the amplitude axis is normalized by the rms amplitude of the pdf

$$A_{\mathrm{rms}} = \sqrt{\int x^2 p_X(x) dx}. \tag{24}$$

The effect of normalization on the echo pdf is demonstrated (Fig. 9). In this illustration, theoretical one-component CF-based echo pdfs of monotype aggregations (see the definition in Section IV-B) composed of varying numbers of scatterers are calculated using (10) and (20), with $N_s = N$ and $N_w = 0$, where N is the number of the only type of scatterer in the aggregations. The predicted curves are normalized according to (24).

Acknowledgment

The authors would like to thank Dr. D. A. Abraham for his suggestions on this paper and providing the code for estimating the parameters of Rayleigh mixture models using an expectation–maximization (EM) algorithm. They would also like to thank the reviewers for their constructive and well-thought comments on this work.

References

[1] F. Le Chevalier, *Principles of Radar and Sonar Signal Processing*. Boston, MA, USA: Artech House, 2002, ch. 6.
[2] T. K. Stanton, "Density estimates of biological sound scatterers using sonar echo peak PDFs," *J. Acoust. Soc. Amer.*, vol. 78, no. 5, pp. 1868–1873, 1985.
[3] T. K. Stanton, "Volume scattering: Echo peak PDF," *J. Acoust. Soc. Amer.*, vol. 77, no. 4, pp. 1358–1366, 1985.
[4] "Special issue on radar clutter," *IET Radar Sonar Navig.*, vol. 4, no. 2, 2010.
[5] "Special issue on non-Rayleigh reverberation and clutter," *IEEE J. Ocean. Eng.*, vol. 35, no. 2, Apr. 2010.
[6] J. W. Goodman, *Statistical Optics*, 1st ed. New York, NY, USA: Wiley-Interscience, 1985, sec. 2.9.
[7] J. Ehrenberg, "A method for extracting the fish target strength distribution from acoustic echoes," in *Proc. IEEE Conf. Eng. Ocean Environ.*, 1972, pp. 61–64.
[8] D. Chu and T. K. Stanton, "Statistics of echoes from a directional sonar beam insonifying finite numbers of single scatterers and patches of scatterers," *IEEE J. Ocean. Eng.*, vol. 35, no. 2, pp. 267–277, Apr. 2010.
[9] M. S. R. Onsrud, S. Kaartvedt, A. Røstad, and T. A. Klevjer, "Vertical distribution and feeding patterns in fish foraging on the krill *Meganyctiphanes norvegica*," *ICES J. Mar. Sci.*, vol. 61, no. 8, pp. 1278–1290, 2004.
[10] B. C. Heezen and C. D. Hollister, *The Face of the Deep*. Oxford, U.K.: Oxford Univ. Press, 1971, ch. 10–13.
[11] D. K. Woolf, "Bubbles and their role in gas exchange," in *The Sea Surface and Global Change*, P. S. Liss and E. R. A. Duce, Eds. Cambridge, U.K.: Cambridge Univ. Press, 1997, ch. 6.
[12] P. Greig-Smith, *Quantitative Plant Ecology*. Los Angeles, CA, USA: Univ. California Press, 1984, ch. 1 and 3.
[13] D. A. Abraham, J. M. Gelb, and A. W. Oldag, "Background and clutter mixture distributions for active sonar statistics," *IEEE J. Ocean. Eng.*, vol. 36, no. 2, pp. 231–247, Apr. 2011.
[14] P. Crowther, "Fluctuation statistics of sea-bed acoustic backscatter," in *Bottom-Interacting Ocean Acoustics*, ser. NATO Conference, W. A. Kuperman and F. B. Jensen, Eds. Boston, MA, USA: Springer-Verlag, 1981, vol. 5, pp. 609–622.
[15] B. R. La Cour, "Statistical characterization of active sonar reverberation using extreme value theory," *IEEE J. Ocean. Eng.*, vol. 29, no. 2, pp. 310–316, Apr. 2004.
[16] T. C. Gallaudet and C. P. de Moustier, "High-frequency volume and boundary acoustic backscatter fluctuations in shallow water," *J. Acoust. Soc. Amer.*, vol. 114, no. 2, pp. 707–725, 2003.
[17] E. Jakeman and P. Pusey, "A model for non-Rayleigh sea echo," *IEEE Trans. Antennas Propag.*, vol. AP-24, no. 6, pp. 806–814, Nov. 1976.
[18] D. Middleton, "New physical-statistical methods and models for clutter and reverberation: The *KA*-distribution and related probability structures," *IEEE J. Ocean. Eng.*, vol. 24, no. 3, pp. 261–284, Jul. 1999.
[19] D. A. Abraham and A. P. Lyons, "Novel physical interpretations of K-distributed reverberation," *IEEE J. Ocean. Eng.*, vol. 27, no. 4, pp. 800–813, Oct. 2002.
[20] K. D. Ward, S. Watts, and R. J. A. Tough, *Sea Clutter: Scattering, The K-Distribution and Radar Performance*. Stevenage, U.K.: IET, 2006, vol. 20, ch. 4.
[21] C. M. Lalli and T. R. Parsons, *Biological Oceanography: An Introduction*. Oxford, U.K.: Butterworth-Heinemann, 1997, ch. 3–6.
[22] K. D. Ward and R. J. A. Tough, "Radar detection performance in sea clutter with discrete spikes," in *Proc. RADAR*, 2002, pp. 253–257, IEE Conf. Publ. No.490.
[23] D. A. Abraham, J. M. Gelb, and A. W. Oldag, "K-Rayleigh mixture model for sparse active sonar clutter," in *Proc. IEEE OCEANS Conf.*, Sydney, 2010, DOI: 10.1109/OCEANSSYD.2010.5603815.
[24] T. K. Stanton and D. Chu, "Non-Rayleigh echoes from resolved individuals and patches of resonant fish at 2–4 kHz," *IEEE J. Ocean. Eng.*, vol. 35, no. 2, pp. 152–163, Apr. 2010.
[25] N. P. Chotiros, "Non-Rayleigh distributions in underwater acoustic reverberation in a patchy environment," *IEEE J. Ocean. Eng.*, vol. 35, no. 2, pp. 236–241, Apr. 2010.
[26] R. Barakat, "First-order statistics of combined random sinusoidal waves with applications to laser speckle patterns," *Optica Acta, Int. J. Opt.*, vol. 21, no. 11, pp. 903–921, 1974.

[27] A. Papoulis, *Probability, Random Variables and Stochastic Processes*, 4th ed. New York, NY, USA: McGraw-Hill, 2002, ch. 5.
[28] D. Abraham, "Signal excess in K-distributed reverberation," *IEEE J. Ocean. Eng.*, vol. 28, no. 3, pp. 526–536, Jul. 2003.
[29] D. Drumheller and H. Lew, "Homodyned-K fluctuation model," *IEEE Aerosp. Electron. Syst. Mag.*, vol. 38, no. 2, pp. 527–542, Apr. 2002.
[30] A. Azzalini, *Statistical Inference Based on the Likelihood*. London, U.K.: Chapman & Hall/CRC Press, 1996, vol. 68, ch. 3.
[31] W. J. Conover, *Practical Nonparametric Statistics*, 3rd ed. New York, NY, USA: Wiley, 1999, ch. 6.
[32] C. D. Sinclair, B. D. Spurr, and M. I. Ahmad, "Modified Anderson Darling test," *Commun. Stat., Theory Methods*, vol. 19, no. 10, pp. 3677–3686, 1990.

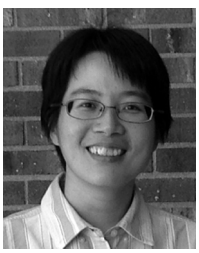

Wu-Jung Lee received the B.S. degree with a double major in electrical engineering and life science (with zoology focus) from National Taiwan University, Taipei, Taiwan, in 2005 and the Ph.D. degree in acoustical oceanography from the Massachusetts Institute of Technology/Woods Hole Oceanographic Institution (MIT/WHOI) Joint Program in Applied Ocean Science and Engineering, Cambridge/Woods Hole, MA, USA, in 2013. Her graduate research focused on broadband and statistical characterization of echoes from random scatterers, inspired in the context of acoustic scattering by marine organisms observed through sonar systems.

She is currently a Postdoctoral Investigator at the Institute for Systems Research, University of Maryland, College Park, MD, USA, working on the biological sonar systems of bats and toothed whales. Her research involves the measurement and modeling of echolocation signals and associated echoes toward understanding the neural computation for auditory scene analysis and sensorimotor integration for active biological sonar systems.

Timothy K. Stanton received the B.S. degree from Oakland University, Rochester, MI, USA, in 1974 and the M.S. and Ph.D. degrees from Brown University, Providence, RI, USA, in 1977 and 1978, respectively, all in physics. His undergraduate research involved experiments in solid-state acoustics with Dr. N. Tepley as advisor and his graduate research involved nonlinear acoustics measurements and instrumentation development with Dr. R. Beyer as advisor.

From 1978 to 1980, he was a Senior Engineer with the Submarine Signal Division, Raytheon Company, Portsmouth, RI, USA, where he was engaged in research, development, and testing of acoustic systems. From 1980 to 1988, he was a Member of the Scientific Staff, Department of Geology and Geophysics, University of Wisconsin, Madison, WI, USA, where he conducted various theoretical, laboratory, and field studies in acoustical oceanography with Dr. C. Clay. From 1988 to the present, he has been a Member of the Scientific Staff, Department of Applied Ocean Physics and Engineering, Woods Hole Oceanographic Institution (WHOI), Woods Hole, MA, USA. From 1997 to 2001, he was Chair of the Department and currently is a Senior Scientist. He currently is collaborating with colleagues in the development of models of acoustic scattering by marine organisms through various theoretical and laboratory methods, physics-based models of the statistics of scattered signals, and is applying the methods to ocean measurements. In addition to his research, he is part of the Massachusetts Institute of Technology (MIT), Cambridge, MA, USA and WHOI Joint Graduate Education Program and teaches acoustic scattering theory. Overall he has published papers covering the areas of nonlinear acoustics, acoustics instrumentation, fiber-optic hydrophones, echo statistics, and acoustic scattering by volumetric objects, seafloor, sea surface, and the underside of sea ice.

Dr. Stanton has served as an Associate Editor for the *Journal of the Acoustical Society of America* and as a Guest Editor for a special issue of *Deep Sea Research*. He has also served as a Guest Editor for a special issue of the IEEE JOURNAL OF OCEANIC ENGINEERING. He is a Fellow of the Acoustical Society of America and is a Member of The Oceanography Society. In 1985, he was awarded the A.B. Wood medal for Distinguished Contributions to Underwater Acoustics